Available online at www.sciencedirect.com
SCIENCE DIRECT®
Materials Research Bulletin 40 (2005) 2225–2242
Materials Research Bulletin
www.elsevier.com/locate/matresbu

Characterization of the thorium phosphate-hydrogenphosphate hydrate (TPHPH) and study of its transformation into the thorium phosphate-diphosphate (β-TPD)

N. Dacheux [a,*], N. Clavier [a,1], G. Wallez [b,2], V. Brandel [a,1], J. Emery [c,3], M. Quarton [b,2], M. Genet [a,1]

[a] *Groupe de Radiochimie, Institut de Physique Nucléaire d'Orsay, Université Paris-Sud-11, Bât. 100, 91406 Orsay, France*
[b] *Laboratoire de Cristallochimie du Solide, Université Pierre et Marie Curie, 4, Place Jussieu, 75252 Paris Cedex 05, France*
[c] *Laboratoire de Physique de l'Etat Condensé, Université du Maine, Avenue O. Messiaen, 72085 Le Mans Cedex, France*

Received 20 January 2005; received in revised form 12 May 2005; accepted 22 June 2005
Available online 18 July 2005

Abstract

The preparation of thorium phosphate-diphosphate ($Th_4(PO_4)_4P_2O_7$, TPD) was developed through the precipitation of thorium phosphate-hydrogenphosphate hydrate ($Th_2(PO_4)_2(HPO_4)\cdot H_2O$, TPHPH) at 150–160 °C in closed PTFE container or in autoclaves. From EPMA analyses and SEM observations, the initial precipitate was single phase and multilayered. The behaviour of TPHPH (orthorhombic system with $a = 21.368(2)$ Å, $b = 6.695(1)$ Å and $c = 7.023(1)$ Å) was followed when heating up to 1250 °C. It was first dehydrated leading to the anhydrous thorium phosphate-hydrogenphosphate (TPHP, orthorhombic system with $a = 21.229(2)$ Å, $b = 6.661(1)$ Å and $c = 7.031(1)$ Å at 220 °C) after heating between 180 and 200 °C. This one turned progressively into the new low-temperature variety of TPD (called α-TPD, orthorhombic system with $a = 21.206(2)$ Å, $b = 6.657(1)$ Å and $c = 7.057(1)$ Å at 300 °C) correlatively to the condensation of hydrogenphosphate groups into diphosphate entities.

* Corresponding author. Tel.: +33 1 69157346; fax: +33 1 69157150.
E-mail addresses: dacheux@ipno.in2p3.fr (N. Dacheux), nclavier@club-internet.fr (N. Clavier), gw@ccr.jussieu.fr (G. Wallez), vbrandel@neuf.fr (V. Brandel), joel.emery@univ-lemans.fr (J. Emery), mq@ccr.jussieu.fr (M. Quarton), migenet2@wanadoo.fr (M. Genet).
[1] Tel.: +33 1 69157346; fax: +33 1 69157150.
[2] Tel.: +33 1 44275544; fax: +33 1 44272548.
[3] Tel.: +33 2 43833291; fax: +33 2 43833518.

0025-5408/$ – see front matter
doi:10.1016/j.materresbull.2005.06.011

These three phases (TPHPH, TPHP and α-TPD) exhibit closely related 2D layered structures, therefore different from the 3D structure of the thorium phosphate-diphosphate (high-temperature variety). This latter compound, now called β-TPD, was obtained by heating α-TPD above 950 °C. All the techniques involved in this study (XRD, Raman and IR spectroscopy, ^{1}H and ^{31}P NMR) confirmed the successive chemical reactions proposed.

Keywords: C. NMR; C. XRD; C. Infrared spectroscopy; C. Raman spectroscopy

1. Introduction

To respond to the French law relative to the radioactive waste management in the field of an underground repository [1], a French National Research group called NOMADE (CEA/CNRS/French universities) was constituted to propose several ceramics for the final disposal of minor actinides (Np, Am, Cm) with weight loadings in actinides up to 10 wt.% and exhibiting normalized dissolution rates, a hundred times lower than those reported for borosilicate glasses of reference [2]. Based on the results obtained about the chemical durability [3–7], the resistance to radiation damage [8,9] and the capabilities of actinides loading [10–13], four matrices were selected [2,14]. They are zirconolite ($CaZrTi_2O_7$) [2], britholites $Ca_{10-x}Nd_x(PO_4)_{6-x}(SiO_4)_xF_2$ [15], monazites $M^{III}PO_4$/brabantites $N^{II}M^{IV}(PO_4)_2$ solid solutions [9,16–18] and thorium phosphate-diphosphate, $Th_4(PO_4)_4P_2O_7$ (TPD) [19].

In this objective, TPD was first prepared for the efficient and specific conditioning of large amounts of tetravalent actinides (up to 47.6 wt.% for uranium) [20–22] and small amounts of trivalent ones (<0.5 wt.%) [23]. The preparation of dense pellets of TPD (and associated thorium-uranium phosphate-diphosphate solid solutions) was also performed with success through a two-step procedure involving an uniaxial pressing at room temperature, then a heat treatment between 1050 and 1250 °C [24].

More recently, the homogeneity of final ceramics was significantly improved by using a new way of preparation based on the precipitation of an initial low-temperature crystallized precursor, $Th_2(PO_4)_2(HPO_4)\cdot H_2O$ (thorium phosphate-hydrogenphosphate hydrate, TPHPH) [25] whose high reactivity allowed to prepare dense pellets for shorter heating times, with associated higher relative densities (92 to 99% of calculated density) and better final homogeneity [26]. Moreover, the very low solubility reported for this precursor ($K_{s,0} \approx 10^{-67}$) [5,7,23] also allowed to consider the quantitative decontamination of low and high level radioactive liquid waste containing actinides (Th, U, Np, Pu) by a new decontamination/precipitation–immobilization chemical process [27,28].

The main aim of this paper is to describe the successive chemical reactions occurring during the transformation of this new low-temperature precursor (TPHPH) into the final ceramic (TPD) considering the results obtained from various physico-chemical techniques like XRD, NMR, IR and μ-Raman spectroscopy, EPMA and TGA/DSC experiments.

2. Experimental

2.1. Synthesis

Chemical reagents, including thorium nitrate pentahydrate, were supplied by VWR, Merck and Aldrich-Fluka. High-temperature treatments were performed up to 1250 °C (with a rate of 5 °C min^{-1})

in alumina boats in air or under inert atmosphere (argon) in a Pyrox HM40 or in an Adamel FR 20 furnace.

As already described in a previously published work [25], TPHPH (of formula $Th_2(PO_4)_2(HPO_4)\cdot H_2O$) was synthesized through two wet chemical routes based on precipitation processes. The first one involved a mixture of thorium nitrate or chloride solution (0.7 M) with 5 M phosphoric acid in the mole ratio $Th/PO_4 = 2/3$, put in a 23 mL PTFE closed container. The gel initially formed was slowly transformed into the crystallized TPHPH when heating at 150–160 °C on a sand bath for several hours. For the second way, the mixture was put in an autoclave set in an oven at 160 °C for about 1 month. Complementary experiments were also performed using other phosphate reagents such as $H_4P_2O_7$ and $(NH_4)_2HPO_4$. The white precipitates were separated from the supernatant by filtration or centrifugation at 4000 rpm, washed several times with deionized water then with ethanol and finally dried at 100 °C for few hours. They were extensively characterized using various techniques.

2.2. Characterization

The Electron Probe MicroAnalyses (EPMA) were carried out using a Cameca SX 50 apparatus working with a 15 kV voltage and a 10 nA current beam. ThO_2 (Mα ray of thorium) and $SmPO_4$ (Kα ray of phosphorus) were used as monitors. These experiments were complicated by the small average grain size observed for several samples. For this reason, 10–50 measurements were performed for each sample then the average values were obtained. SEM micrographs were performed with a Hitachi S2500 scanning electron microscope.

Thermogravimetric analysis (TGA) and differential thermal analysis (DTA) experiments were done with a Setaram TG 92-16 apparatus under dry argon atmosphere with a heating rate from 0.05 to 1 °C min^{-1} (TGA) or from 2 to 5 °C min^{-1} (DTA). The rough values of the weight losses obtained by TGA were corrected from the Archimedes buoyancy. DSC measurements were carried out in flowing dry argon with a Setaram CS 92 apparatus with heating rate of 5 °C min^{-1}. All the sample weights were in the range of 20–40 mg.

At room temperature, the precise powder diffraction data were collected with a Siemens D5000 high-resolution diffractometer. The alignment of the instrument was checked by means of the 0 0 *l* reflections of fluorophlogopite mica (NIST SRM 675) [29]. From 20 to 300 °C, the XRD were obtained with a Philips PW 1050/25 goniometer equipped with a heating holder Anton Paar TTK. The high-temperature XRD (HT-XRD) were recorded with a Philips X'PERT-PRO-PW 3040/60 goniometer for heating temperatures up to 1100 °C under nitrogen atmosphere using an Anton Paar HTK 1200 furnace. The diffraction patterns were taken between 5 and 60° (2θ) with a step of 0.02°, using monochromatized Cu Kα radiation ($\lambda = 1.54060$ Å). The refinement of the unit-cell parameters was performed by Rietveld method in profile-matching mode, using the Fullprof.2k program [30]. Instrumental data (Voigt coefficient, peak width and asymmetry polynomials) were fixed as previously refined from an Al_2O_3 pattern. The variables were the cell parameters, the 2θ shift, the four coefficients of the background polynomial and a (1 0 0) axial micro-strain parameter.

Infrared absorption spectra were recorded from 400 to 4000 cm^{-1} using cylindrical pellets ($\varnothing = 10$ mm) of about 1 wt.% of sample in KBr with an Hitachi I-2001 spectrophotometer. The in situ (performed at the studied temperature up to 300 °C) and ex situ (performed at

room temperature) Raman spectra were recorded using a Labram (Dilor-Jobin Yvon) microspectrometer with an argon laser working at 514.5 nm and equipped with a Notch filter. The power varied from 1 to 10 mW on the samples and the laser beam was focused on the sample with an Olympus microscope.

One and two dimension nuclear magnetic resonance investigations (1D and 2D, respectively) were also used. The NMR spectra were recorded with a Bruker Avance 300 spectrometer working at $\nu_0 = 121.494$ MHz for ^{31}P (experimental parameters reported in Table 1). In a first step, magic angle spinning (MAS) (1D) one pulse experiments were performed on ^{31}P. Eight transients were accumulated. The delay between two successive transients was taken at 800 s to obtain quantitative 1D spectra and to take into account the ^{31}P relaxation time which is between 35 and 80 s.

Two types of double quanta (DQ) experiments were carried out with a MAS rotation frequency of 10 kHz. For ^{31}P (spin 1/2), DQ signal observation corresponds to two coupled nuclei. Only one quantum (1Q) signal was physically observed and DQ signal was indirectly observed in a supplementary dimension (2D experiments). In the DQ experiments, the DQ coherences evolved after they were excited, then are reconverted before being observable. The first DQ experiment uses the dipolar re-coupling (through space) [31–34] while the second involves the J (through bond) coupling. In the dipolar case, the DQ are excited and reconverted by using the POST-C7 sequence [34]; the J coupling was realized with the well known incredible natural abundance double quantum transfer experiment (INADEQUATE) sequence [35]. The 2D diagram correlates double quantum dipolar spectrum (or J spectrum) in the F1 dimension (vertical axis) and single quantum ^{31}P MAS spectrum in the F2 dimension (horizontal axis) which allowed to establish the connectivity between the different phosphorus. By exciting the DQ, these experiments allow to evidence the phosphorus nuclei which are coupled either through space by the dipolar interaction or through bonds by the J interaction which can bring information on the presence of P_2O_7 groups. Owing to the long spin lattice relaxation time T_1, before each transient in the 2D double quantum spectrum, the sequence begins with a saturation pulse train and the delay between transient is lowered at 30 s. The use of low delay leads to the enhancement of impurity lines with small T_1. So, some peaks, not observed in 1D experiments with long delay, become more important and could appear in the 2D experiments.

Table 1
Experimental parameters for the NMR study

Parameter	1D experiment	2D experiment
Pulse length (μs)	3.57	
Dead time (μs)	10	
Recycle time (s)	800	30
Resonance frequency (MHz)	121.494	
MAS spinning speed (kHz)	10	
Number of transients	8	48
Number of digitized points	1024	196
Reference used	15 M H_3PO_4	

The $\pi/2$ pulse length corresponds to an amplitude radio frequency field of 70 kHz which is seven times the MAS frequency spinning used in the POST-C7 experiment.

3. Results and discussion

3.1. Characterization of TPHPH

From EPMA experiments (Table 2), all the powdered samples of $Th_2(PO_4)_2(HPO_4)\cdot H_2O$ appeared homogeneous and single phase. Moreover, the elementary weight percents as well as the corresponding Th/P mole ratios (i.e. 2/3) were found to be in good agreement with the expected empirical formula.

Whatever the initial phosphate reagent considered (either H_3PO_4, $H_4P_2O_7$ or $(NH_4)_2HPO_4$), the same compound was precipitated, even using diphosphoric acid. A small variation of the initial stoichiometric conditions (e.g. 10 mol% of excess or default of phosphate) did not influence the stoichiometry of the precipitate. From phosphoric acid, the following chemical reaction of precipitation of TPHPH can be proposed:

$$2Th^{4+} + 3H_3PO_4 + 9H_2O \rightarrow Th_2(PO_4)_2(HPO_4)\cdot H_2O\downarrow + 8H_3O^+ \quad (1)$$

The IR and Raman spectra of TPHPH, prepared at 160 °C exhibited both O–H stretching and H–O–H bending vibrations as described in the literature [36–38]. The large band at 3412 cm^{-1} can be assigned to the O–H stretching vibrations while the band located at 1630 cm^{-1} corresponds to the bending mode of H_2O. Considering the studies of several phosphate compounds mentioned in the literature [39–42], the vibrations of the P–O bonds are observed from 340 to 450 cm^{-1} (δ_s), from 500 to 630 cm^{-1} (δ_{as}), from 960 to 1000 cm^{-1} (ν_s) and from about 1000 to 1160 cm^{-1} (ν_{as}) in the infrared and μ-Raman spectra of TPHPH (see Table 4). Moreover, as already described, the observation of two shoulders at about 3200 and 2400 cm^{-1}, in the IR spectra of TPHPH, can be associated to the (P)–O–H stretching modes while the intense bands located near to 1250 cm^{-1} (IR) and near to 880–940 cm^{-1} (IR and Raman) could be attributed to the deformation of P–O–(H) in the plane (δ_{ip}) and out of plane (δ_{op}), respectively [36,43–47]. All these results seem to confirm the presence of hydrogenphosphate groups and to exclude that of P_2O_7 entities as it was strongly suggested by NMR experiments [48].

Indexing of the XRD patterns of TPHPH was performed using the program DICVOL91 [49] from the first 20 lines. The unique orthorhombic solution was checked by reviewing the complete data by means of the evaluation program NBS*AIDS83 [50]. The refined unit-cell parameter values were found to be $a = 21.368(2)$ Å, $b = 6.695(1)$ Å and $c = 7.023(1)$ Å, i.e. $V = 1004.8(4)$ $Å^3$. The corresponding experimental density, determined by water and/or helium pycnometry, $\rho_{exp.} = 5.02(5)$, was in good agreement with the calculated value, $\rho_{cal.} = 5.077$ for $Z = 4$ unit formula per cell.

From scanning electron microscopy, the powders appear as agglomerated circular small plates (Fig. 1). The electron diffraction revealed that the main plane of these small plates corresponds to (b, c). Thus, the grain morphology seems to indicate a 2D-structure parallel to the (1 0 0) plane.

Table 2
EPMA results obtained for TPHPH: $Th_2(PO_4)_2(HPO_4)\cdot H_2O$

Phosphating reagent	Th (wt.%)	P (wt.%)	Th/P
Calculated	60.4	12.1	0.67
H_3PO_4	60.4 ± 0.5	12.4 ± 0.1	0.65 ± 0.01
$H_4P_2O_7$	61.3 ± 0.5	12.1 ± 0.2	0.67 ± 0.02
$(NH_4)_2HPO_4$	61.2 ± 0.4	12.1 ± 0.2	0.67 ± 0.02

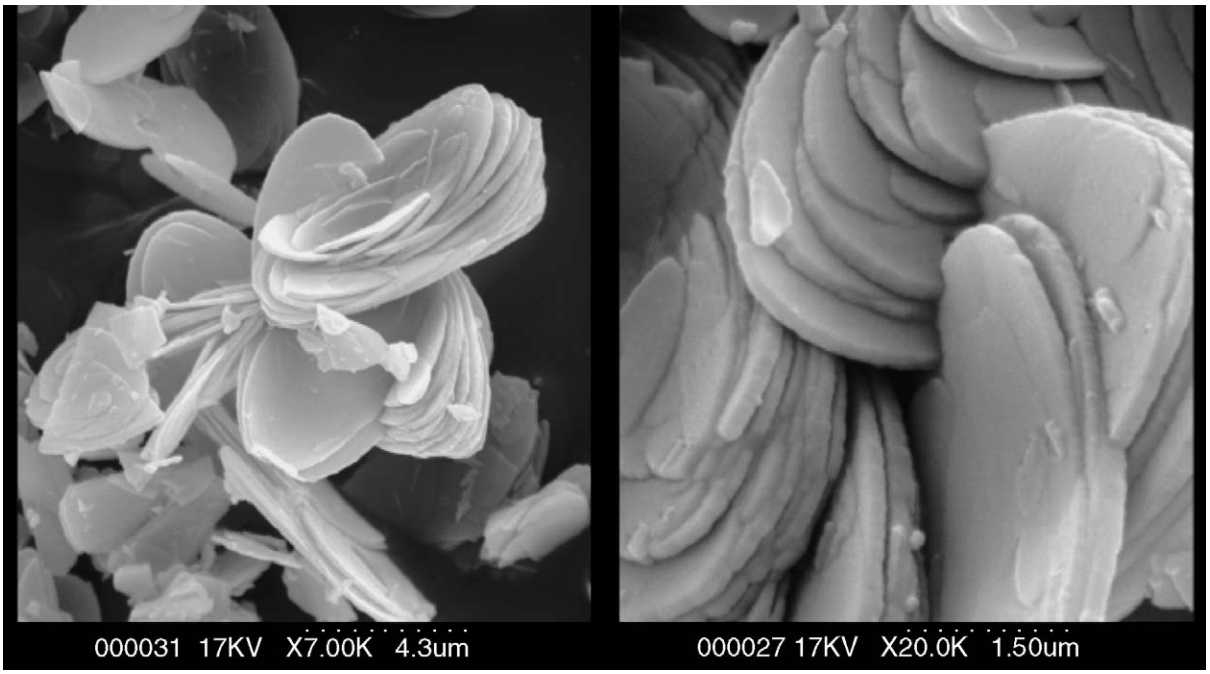

Fig. 1. Scanning electron micrographs of TPHPH prepared in closed container on a sand bath at 160 °C for 3.5 h.

3.2. Behaviour of TPHPH versus temperature

The DTA analysis recorded with a heating rate of 5 °C min^{-1} exhibited three thermal incidents (Fig. 2): two endothermic peaks (a strong peak at 225 °C and a shoulder at 256 °C) and one exothermic around 950 °C. In the same range of temperature, TGA showed a total weight loss of 3.6% between 190 and 270 °C corresponding to the endothermic phenomenon. Likewise, DSC experiments performed in the same conditions gave two peaks at 236 and 265 °C, with a total variation of enthalpy of 93.2 J g^{-1}. In order to identify the nature of the endothermic incidents, TGA was repeated with a slower heating rate (0.1 °C min^{-1}) (Fig. 3). This allowed to observe two separate phenomena between 180 and 210 °C (weight loss of 2.3%) and between 210 and 280 °C (weight loss of 1.2%), instead of the previous one (3.6%). Insofar as the weight ratio of a water molecule in TPHPH corresponds to 2.34% calculated, it can be assumed that the first peak corresponds to the full dehydration of TPHPH into $Th_2(PO_4)_2(HPO_4)$ (TPHP) and the shoulder, to the additional loss of 0.5 water molecule resulting from the condensation of two HPO_4 groups leading to one diphosphate entity. Thus, through the condensation of two hydrogenphosphate groups, TPHPH yields to the low-temperature form of $Th_4(PO_4)_4P_2O_7$ (α-TPD) above 280 °C which turns into β-TPD (high-temperature form) near to 950 °C through an irreversible phase transition.

Prior to the complete characterization of the samples, electron probe microanalyses were performed for several temperatures of calcination. The results confirmed that, for all the heating temperatures considered, the samples remained homogeneous and single phase (Table 3). Moreover, the elementary weight percentages were in good agreement with those expected taking into account both formula $Th_2(PO_4)_2(HPO_4)\cdot H_2O$ and α-$Th_4(PO_4)_4P_2O_7$. However, while the composition was found to be consistent with that of

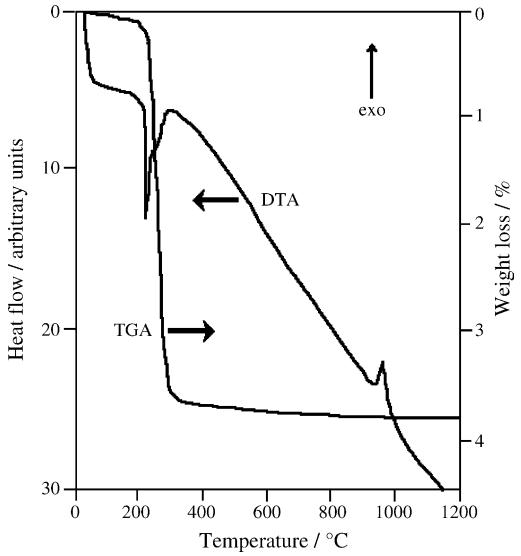

Fig. 2. DTA–TGA curves recorded from TPHPH (heat rate of 5 °C min^{-1}).

TPHPH for the raw sample, it seems to reach that of α-TPD (or β-TPD) above 400 °C. In the whole temperature range studied, the Th/P mole ratio remained unchanged (average value of 0.67) which agreed well with the stoichiometry of the chemical formulae proposed and confirmed that the phosphate anion was not eliminated by volatilization of phosphorus (V) oxide during the heat treatment.

In order to confirm the chemical steps occurring during the transformation of TPHPH into β-TPD, high-temperature XRD diagrams and high-temperature μ-Raman spectra (HT-Raman) were recorded from room temperature to 1175 and 300 °C, respectively. Complementary IR and Raman experiments were also carried out at room temperature on samples previously heated between 400 and 1250 °C.

3.3. HT-XRD study

HT-XRD diagrams were carried out from 20 to 1250 °C with intervals of 50 °C and 30 min steps in order to characterize the new TPHP and α-TPD phases resulting from water loss of the heated TPHPH

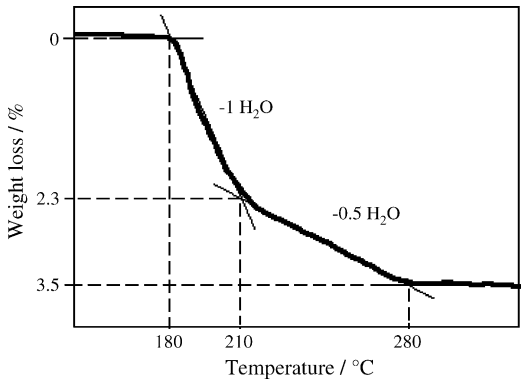

Fig. 3. TGA curve recorded from TPHPH (heating rate of 0.1 °C min^{-1}).

Table 3
EPMA results obtained for several samples heated at various temperatures

	Th (wt.%)	P (wt.%)	Th/P
Calculated[a]	60.4	12.1	0.67
Calculated[b]	61.9	12.4	0.67
Room temperature	60.4 ± 0.5	12.4 ± 0.1	0.65 ± 0.01
400 °C	61.7 ± 0.8	12.3 ± 0.4	0.67 ± 0.03
600 °C	61.8 ± 0.6	12.3 ± 0.3	0.68 ± 0.02
800 °C	62.3 ± 0.5	12.0 ± 0.2	0.69 ± 0.02
1250 °C	62.2 ± 0.3	12.6 ± 0.1	0.67 ± 0.01

[a] Calculated considering the formula $Th_2(PO_4)_2(HPO_4)\cdot H_2O$.
[b] Calculated considering the formula $Th_4(PO_4)_4P_2O_7$.

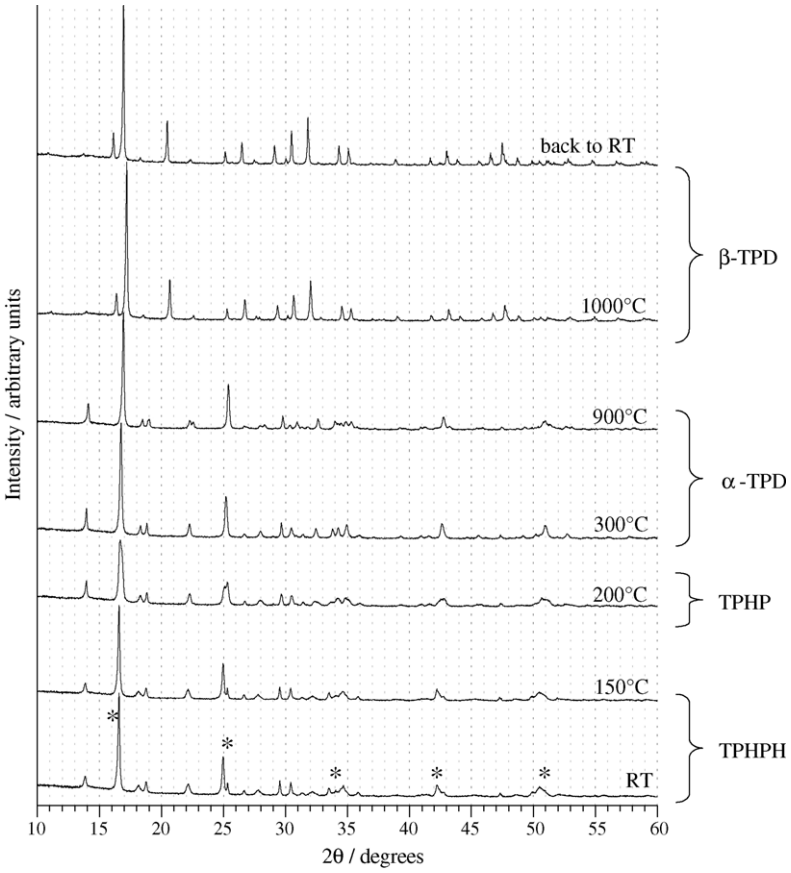

Fig. 4. HT-XRD diagrams recorded for various temperatures starting from TPHPH (variation from TPHPH to β-TPD via the formation of TPHP then α-TPD). The XRD lines corresponding to the ($h = 2n$, 0, 0) family are marked by asterisks.

sample. They revealed that the diagram of TPHPH was not significantly modified between room temperature and 900 °C (Fig. 4). However, a small shift of $h\,0\,0$ peaks to the upper angles (400, 600 and 800 at $2\theta = 16.6$, 25.0 and 33.5°, respectively) was observed between 180 and 250 °C and was correlated to their significant broadening (which was found to be maximum between 180 and 210 °C, that is to say during the departure of crystallization water).

The thermal variations of the unit-cell parameters exhibit several irregularities which are correlated to the phase transitions (Fig. 5). Several domains must be considered.

- Below 180 °C, the variations remain weak while no chemical transformation occurs.
- From 180 to 220 °C, the a and b unit-cell parameters decrease while the c variation is negligible: TPHPH dehydrates with a net volume drop (the mean value $\Delta l/l_0$ decreases). The unit-cell parameters for the resulting TPHP formed at 220 °C are:

$$a = 21.229(2)\,\text{Å}\ , \quad b = 6.661(1)\,\text{Å} \quad \text{and} \quad c = 7.031(1)\,\text{Å}\ , \quad \text{i.e. } V = 994.2(4)\,\text{Å}^3.$$

- From 220 to 300 °C, the a and b parameters decrease slowly, while c increases rapidly: HPO_4 groups are transformed into P_2O_7 entities by condensation, with the loss of additional 0.5 H_2O per unit formula and a very small volume increase is observed. The unit-cell parameters for the resulting α-TPD, prepared at 300 °C, are:

$$a = 21.206(2)\,\text{Å}, \quad b = 6.657(1)\,\text{Å} \quad \text{and} \quad c = 7.057(1)\,\text{Å}\ , \quad \text{i.e. } V = 996.2(4)\,\text{Å}^3.$$

- Above 300 °C, the weak variations are regular and globally positive.

Between 300 and 950 °C, the XRD was kept unchanged until the β-form of TPD was obtained. Above this temperature, only the diffraction lines of β-TPD were observed, excluding the presence of secondary phases such as $Th_2(PO_4)(P_3O_{10})$ reported in literature [51], α-ThP_2O_7 or ThO_2. As expected, β-TPD was

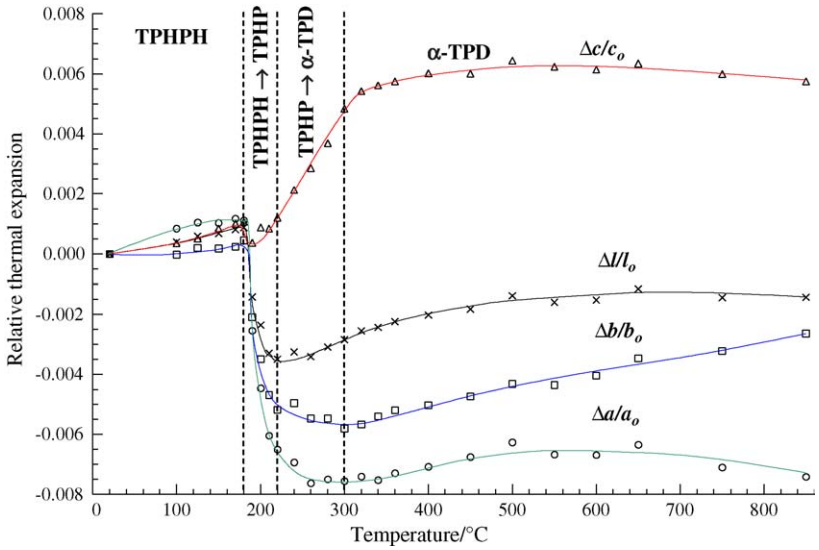

Fig. 5. Relative thermal variations of the three unit-cell parameters ($\Delta l/l_0$ is the mean value) obtained by HT-XRD from 20 to 850 °C (the error bars representing standard deviations are comparable in dimensions with the symbols used).

found to be stable up to 1300 °C. Above this temperature, it was slowly decomposed into the thoryl phosphate $(ThO)_3(PO_4)_2$ and thorium dioxide ThO_2, as already described in literature [19,52].

The thermal variations of the cell edges are nevertheless moderate and continuous. This accounts that these three phases (TPHPH, TPHP and α-TPD) have very similar structures. Thus, we can conclude that the water molecules and the protons fixed on some phosphate groups in TPHPH do not play a significant steric or structural role insofar as the most prominent effect of their loss corresponds to a moderate reduction of the *a*-parameter (−0.7%). This accounts for the 2D-character of the TPHPH structure, which is supposed to host water molecules and protons in the interlayer spaces.

3.4. Infrared and μ-Raman spectroscopies

Several μ-Raman (HT-Raman) spectra were recorded between room temperature and 300 °C (Fig. 6). Complementary Raman and IR spectroscopy experiments were carried out, at room temperature, on samples previously heated between 250 and 1250 °C (Figs. 7 and 8, respectively). The HT-Raman spectra, recorded between room temperature and 300 °C (Fig. 6) exhibited some significant modifications between both temperatures. Indeed, the symmetric stretching mode of the P–O–P bridge (located near 770–780 cm^{-1}) [53–55], characteristic of diphosphate groups, is absent on the spectra of TPHPH

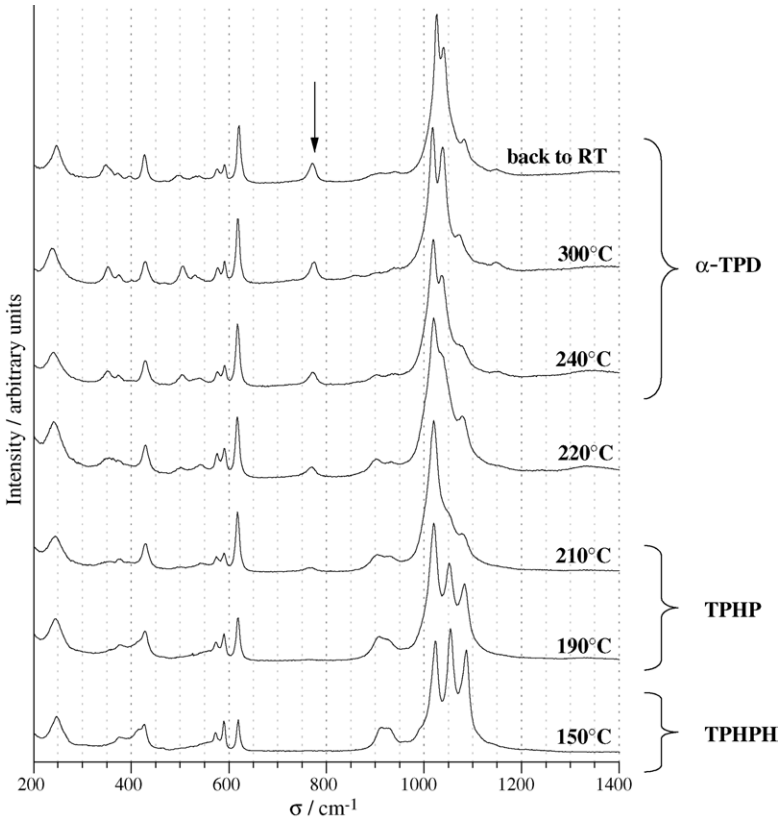

Fig. 6. HT-Raman spectra recorded from TPHPH for various temperatures of calcination. The arrow points out the characteristic ν_s(P–O–P) vibration band.

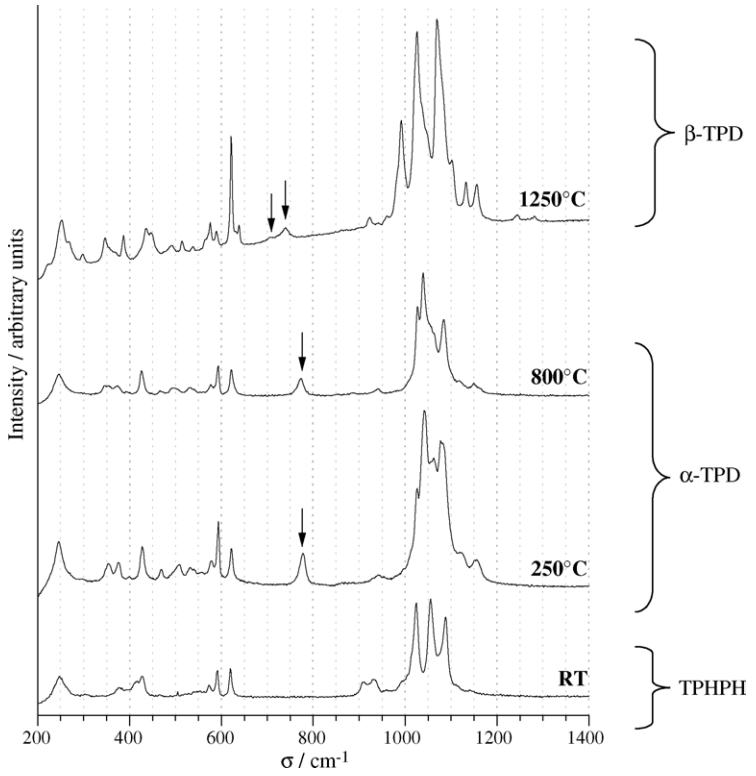

Fig. 7. RT-Raman spectra of TPHPH and after heating the sample at several temperatures. The arrows point out the characteristic ν_s(P–O–P) vibration band.

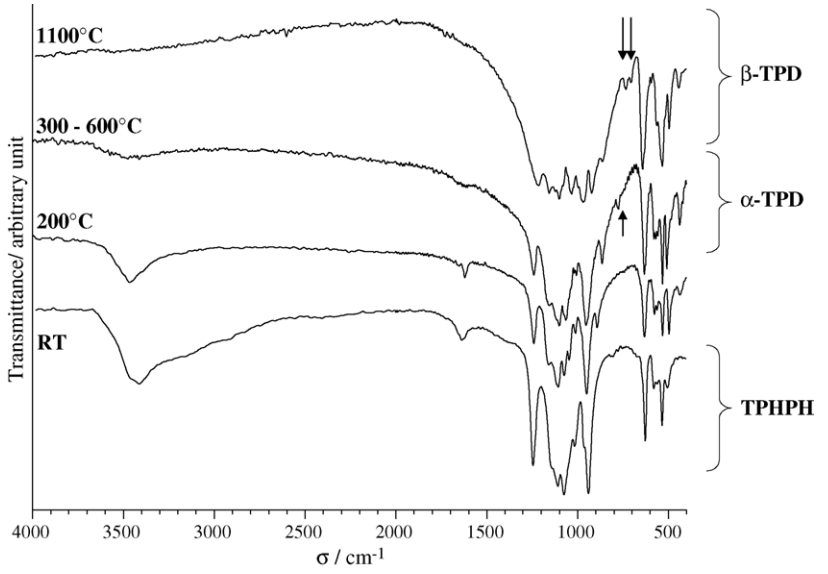

Fig. 8. Variation of the IR spectra from TPHPH to β-TPD recorded at room temperature on samples heated at several temperatures.

and TPHP, and weakly appears when heating the sample above 200 °C. Its intensity becomes more significant on the Raman spectra recorded at 210–220 °C (Fig. 6) and seems to be unchanged above 250 °C. In these conditions, the transformation of HPO_4 groups into P_2O_7 entities seems to be progressive and spreads from 210 to 250 °C. The band associated to the ν_s(P–O–P) vibration is still present on room-temperature Raman spectra of samples previously heated at 250 or 800 °C (Fig. 7). When β-TPD is formed (above 950 °C), this band is split in two components at 705 and 741 cm^{-1} in the Raman spectrum (Fig. 7) and at 706 and 734 cm^{-1} in the IR spectrum (Fig. 8), as already described for pure β-TPD prepared by direct evaporation or by dry chemistry methods [19]. The proposed assignment of the vibration bands is given in Table 4.

Correlatively to the appearance of the absorption bands assigned to the ν_s(P–O–P) and ν_{as}(P–O–P) vibrations, the μ-Raman and IR spectra become more complicated and less resolved when heating the samples above 210 °C, probably due to the coexistence of PO_4 and P_2O_7 groups. Especially, additional bands are observed near 350, 470, 505 and 530 cm^{-1} (triplet) and between 1120 and 1155 cm^{-1} in the Raman spectra recorded above 210 °C. They were located at 348 cm^{-1} and at 490, 515 and 538 cm^{-1} in the Raman spectrum of the final β-TPD (Fig. 7, θ = 1250 °C). The coexistence of PO_4 and P_2O_7 groups, above 210 °C, could explain the six bands in the domains of δ_{as} and ν_{as} vibrations (i.e. 470–640 and 1000–1175 cm^{-1}, respectively) instead of the three expected for each type of vibration (three-fold vibration modes in the C_{2v} or C_2 symmetry for δ_{as} and ν_{as}). Moreover, the observation of different grains between 200 and 250 °C confirmed that the transformation was not homogeneous and very progressive. Indeed, in the same sample (HT-Raman spectra recorded at 210 °C), some grains correspond to the remaining TPHP while others already exhibit the absorption bands of the P_2O_7 groups. Moreover, this transformation was found to be irreversible since the ν_s (P–O–P) vibration band remained still present in the room-temperature μ-Raman spectrum of the sample previously heated up to 300 °C. Two additional bands, located between 1240 and 1280 cm^{-1} (very weak) were present in the μ-Raman and at 1220 cm^{-1} in the

Table 4
Assignment of the IR and Raman bands (cm^{-1}) for samples heated at various temperatures

	δ_s(P–O)	δ_{as}(P–O)	ν_s(P–O–P)	ν_{as}(P–O–P)	ν_s(P–O)	ν_{as}(P–O)	δ_{op}(P–O–(H)) δ_{ip}(P–O–(H))
Raman							
T = 25 °C	360–430	560–620	–	–	957, 1000	1025–1140	910, 935
T = 150 °C[a]	350–440	560–640	–	–		1015–1100	909, 922
T = 210 °C[a]	345–450	490–630	767	904–930		1020–1105	–
T = 250 °C[a]	350–430	470–625	778	940	997	1025–1155	–
T = 800 °C	345–425	470–620	773	940	N.O.[c]	1025–1150	–
T = 1250 °C	345–450	490–640	705, 741	922, 942	960	990–1280	–
IR							
T = 25 °C	439	500–625	–	–	962	1005–1105	934, 1251
T = 25 °C[b]	437	505–630	–	–		1010–1125	936, 1242
T = 300 °C	438	500–630	772	945	994	1000–1175	891, 1252
T = 400 °C	438	500–630	768	943, 961	–	1010–1180	887, 1252
T = 1100 °C	444	496–644	706, 734	922	970	1000–1220	–

[a] HT-Raman spectrum.
[b] Prepared from $H_4P_2O_7$.
[c] N.O.: not observed.

IR spectra of β-TPD (Figs. 7 and 8) and could be correlated to the ν_{as} (P–O) vibration influenced by adjacent Th–O edges.

The bands associated to the P–O–(H) edge in the plane deformation and/or to vibrations associated to water molecules adsorbed on phosphate layers were still present in the spectrum of TPHP obtained after heating at 200 °C as well as the bands corresponding to O–H and H_2O vibrations, probably due to the hygroscopic properties of the solid. However, the intensity of the absorption bands corresponding to water molecule decreased significantly above 200 °C. In order to check this hypothesis, two TPHPH samples were heated in air for 1 h at 200 and 400 °C, then left at room temperature for 3 h. When heated again, the weight loss was the same for both samples (about 2%), according to the fact that both TPHP and α-TPD are prone to water adsorption which was already observed for anhydrous hydrogenphosphates [56,57]. Moreover, the IR and Raman spectra of samples heated between 300 and 800 °C revealed the presence of weak bands of the O–H and H–O–H vibrations which is rather surprising for this range of temperature. This observation was assigned to water molecules adsorbed onto the surface of the sample (hygroscopic behaviour of the samples).

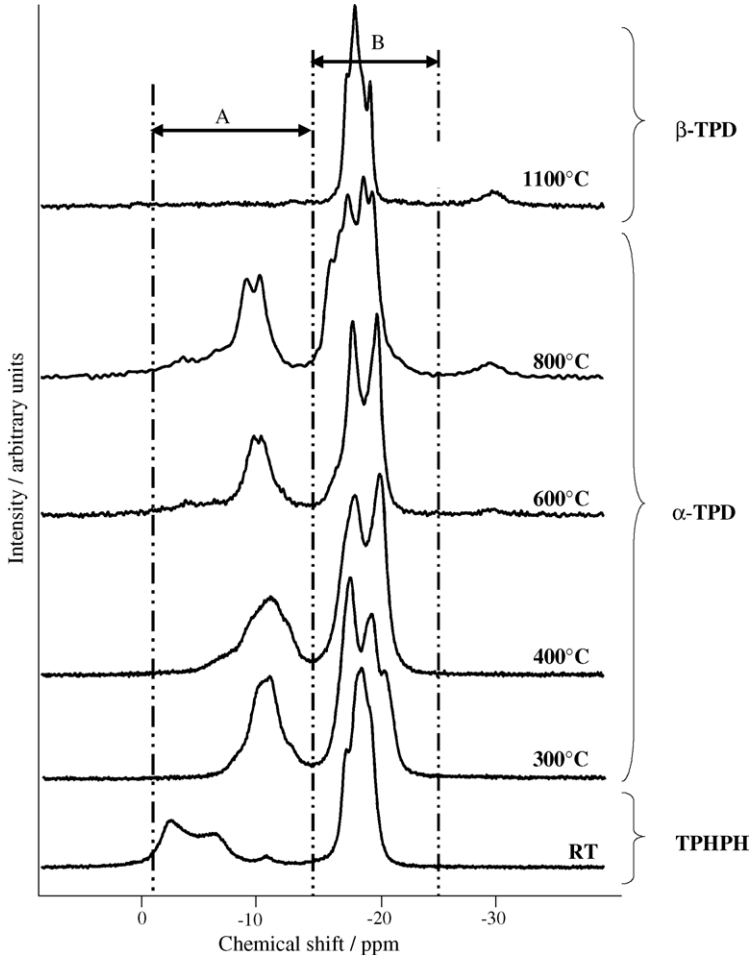

Fig. 9. Variation of ^{31}P NMR spectra from TPHPH to β-TPD. The spectra evidence two domains named A and B.

3.5. NMR study

NMR experiments were performed at room temperature on TPHPH and on samples heated at 300, 400, 600, 800 and 1100 °C for 12 h under inert atmosphere [48,58] prior to perform the NMR experiments. The corresponding ^{31}P NMR MAS spectra are gathered in Fig. 9. Except for the sample prepared at 1100 °C, the ^{31}P spectrum consists in two blocks of lines named A (at low field, short spin lattice relaxation time $T_1 = 35$ s) and B (located at high field, long T_1 value: $T_1 = 80$ s) which variations were followed versus the heating temperature. The weak band between A and B (at −11 ppm) in the TPHPH spectrum, was assigned to an impurity. It is worth to note that, for all the temperatures considered (except for $T = 1100$ °C), the relative areas of both A- and B-blocks remained constant (with the ratio 1/3 for A and 2/3 for B) which appears in good agreement with both formula $Th_2(PO_4)_2(HPO_4)\cdot H_2O$ and $Th_4(PO_4)_4P_2O_7$. The number of lines in the B-block was found between two and four depending on the sample. This was assigned to the readsorption of water molecules during the cooling step (hygroscopic behaviours of both TPHP and α-TPD) which made the phosphorus atoms equivalent or not. Nevertheless, the lines observed in the B domain were always found between −16 and −20 ppm. On the other hand, the lines of the A-block which were observed between −3 and −7 ppm in TPHPH were shifted toward the high field (−8 ppm/−12 ppm) for the other samples heated above 300 °C indicating some significant modifications in the nature of the phosphorus nuclei of the A-block.

The through space (dipolar interaction) spectrum (Fig. 10) shows that the phosphorus nuclei of the two massifs A and B are coupled as given by the inter-correlation peaks (A–B) in TPHPH and in α-TPD which confirms that there is no phase separation in these samples.

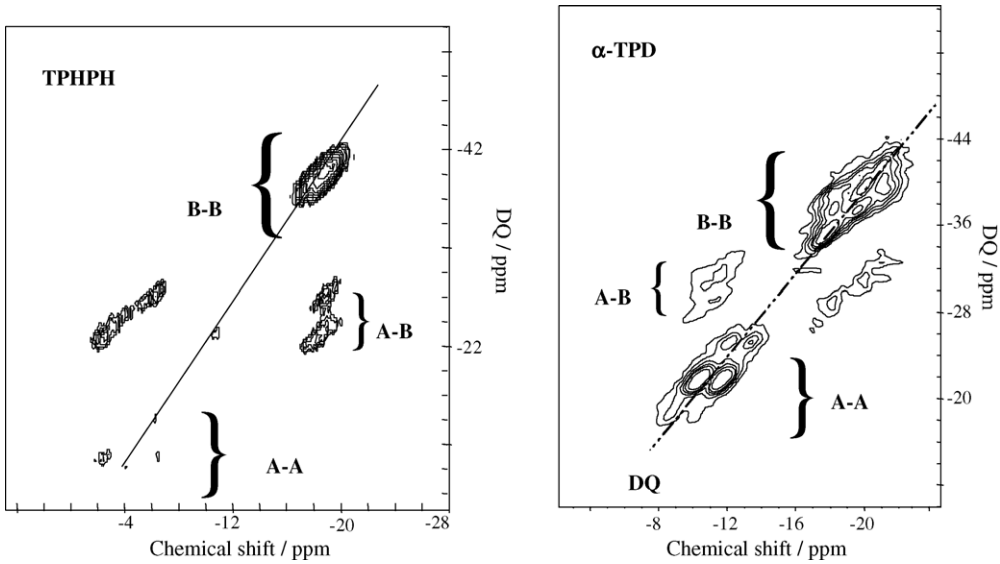

Fig. 10. Through space correlation experiments for TPHPH and α-TPD (prepared after heating TPHPH at 300 °C). In TPHPH, no correlation appears in the massif A while they exist in α-TPD. The correlation between the phosphorus nuclei of the domains A and B are clearly evidenced in both samples. The line corresponds to the double quantum diagonal.

In TPHPH, either auto- and inter-correlation between the phosphorus nuclei in the A-block were found to be very weak (or non existent) in the through space experiment (dipolar coupling) (Fig. 10) or absent from the INADEQUATE data (Fig. 11) which means that the phosphorus nuclei of the A-block are not chemically coupled, excluding the presence of P_2O_7 entities in TPHPH.

On the contrary, the data obtained on α-TPD differed significantly from the previous one. Indeed, some correlation peaks in the A-zone are observed either in through space (Fig. 10) or through the bond coupling (Fig. 11), which means that the J coupling and dipolar coupling between phosphorus atoms is active in this solid. Thus, the phosphorus atoms of the A-massif, which were found to be independent in TPHPH, becomes bounded confirming the condensation of HPO_4 groups into P_2O_7 entities in α-TPD. In α-TPD, phosphorus nuclei in the A-domain associated to the P_2O_7 entities are not structurally equivalent (two different lines) in opposition with that was observed in β-TPD [48,58]. It is worth to note that the B–B couplings observed in the through bond experiment in TPHPH and α-TPD disappear when the MAS rotation frequency is higher. The appearance of the diagonal peaks are due to rotational resonance effect. The peaks out of the diagonal come from entities with small T_1 and are enhanced due to the small delay between transients (30 s instead of 800 s) used in the 2D experiments. It is important to note that the spin lattice relaxation times are 35 and 80 s for the most intense peaks.

Thus, the INADEQUATE experiment clearly shows that the phosphorus of the A-block are not coupled through chemical bond in TPHPH and do not correspond to phosphorus nuclei of P_2O_7 entities (otherwise the through space experiment could give large correlation peak). This result also confirms the conclusion obtained with the REDOR and CPREDOR experiments [58]: there is no P_2O_7 group in TPHPH and the A-massif corresponds to phosphorus involved in HPO_4 groups [58]. The phosphorus nuclei of the A-block are the most sensitive in the CP-MAS [48] experiment and correspond to the shortest distance 2.1 Å which is in the range of d (P–O) + d (O–H) ≈ 2.6 Å in HPO_4 entities (for a bond angle P–O–H of about 120°).

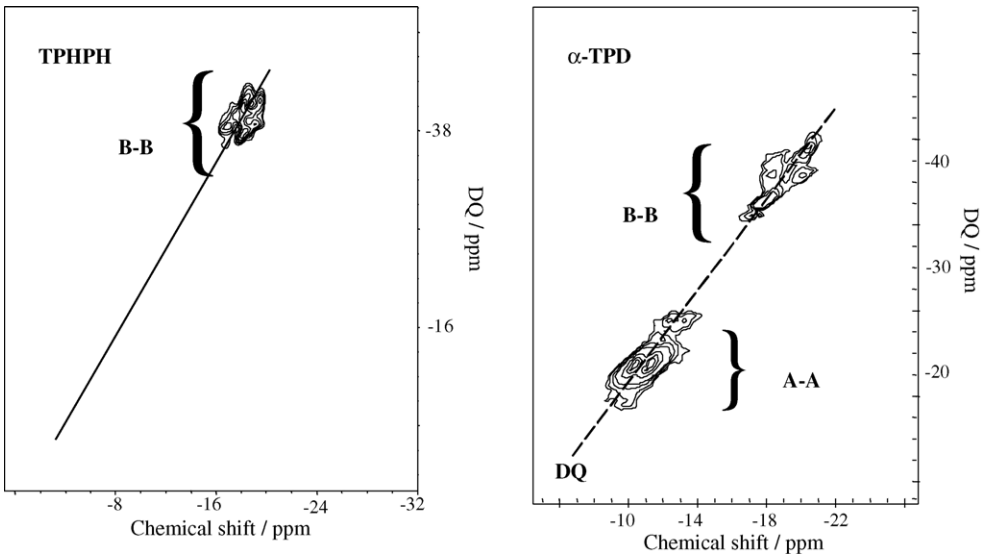

Fig. 11. Through bond correlation experiments for TPHPH and α-TPD (prepared after heating TPHPH at 300 °C). In TPHPH, no correlation appears in the A-massif while they exist in α-TPD. The line corresponds to the double quantum diagonal.

4. Conclusions

Well-crystallized TPHPH was synthesized through two wet chemical routes in closed containers. EPMA experiments confirmed that the samples were homogeneous and single phase. Between 180 and 220 °C, TPHPH was fully dehydrated leading to the anhydrous thorium phosphate-hydrogenphosphate (TPHP). XRD, NMR studies and TGA/DSC experiments, on the one hand, and IR and Raman spectroscopies, on the other hand, evidenced that TPHP was progressively transformed above 220 °C into the low-temperature form of the thorium phosphate-diphosphate (α-TPD). This transformation was progressive and spread from 220 to 300 °C. The presence of P_2O_7 groups was clearly established for samples heated above 200 °C. The α-TPD was converted into β-TPD (high-temperature form) by heating above 950 °C, in air or under inert atmosphere. By this way, well-crystallized, pure and homogeneous samples of β-TPD were prepared.

The three phases (TPHPH, TPHP and α-TPD) exhibit close related 2D layered structures. The main differences result from the presence of water molecules (in TPHPH) and protons (in TPHPH and in TPHP) in the interlayer spaces, which do not belong to the structural framework. The loss of the latter goes together with the condensation of the hydrogenphosphate groups:

$$2HPO_4^{2-} \rightarrow P_2O_7^{4-} + H_2O\uparrow \quad (2)$$

As a summary, the following scheme of preparation of β-TPD from TPHPH can be proposed:

$$2Th_2(PO_4)_2(HPO_4)\cdot H_2O \xrightarrow{180^\circ C \le T \le 220^\circ C} 2Th_2(PO_4)_2(HPO_4) + 2H_2O\uparrow \quad (3)$$

$$2Th_2(PO_4)_2(HPO_4) \xrightarrow{220^\circ C \le T \le 300^\circ C} \alpha\text{-}Th_4(PO_4)_4P_2O_7 + H_2O\uparrow \quad (4)$$

then finally:

$$\alpha - Th_4(PO_4)_4P_2O_7 \xrightarrow{T \ge 950^\circ C} \beta\text{-}Th_4(PO_4)_4P_2O_7 \quad (5)$$

The sequence of the reactions is now clearly demonstrated. No significant decomposition of β-TPD was observed up to 1300 °C as confirmed from TGA and DTA as well as from XRD and EPMA experiments.

Acknowledgements

The authors would like to thank Renaud Podor, Johann Ravaux, Lionel Aranda, Jean-Paul Emeraux and Alain Kohler from the LCSM of the University Henri Poincaré of Nancy (France) for the EPMA experiments, the TGA/DTA experiments and the SEM observations. They would like to thank Thérèse Lhomme from the CREGU (University of Nancy) for performing μ-Raman experiments and Jean-Paul Souron (University of Paris VI) for DSC and XRD measurements.

Reference

[1] J.C. André, C.R. Acad. Sci. Paris-IIA 333 (2001) 835–839.
[2] X. Deschanels, in: Evaluation de la faisabilité Technique des nouvelles matrices de conditionnement des radionucléides à vie longue, Technical report CEA, DTCD/2004/5, 2004.

[3] F. Poitrasson, E.H. Oelkers, J. Schott, J.M. Montel, Geochim. Cosmochim. Acta 68 (2004) 2207–2221.
[4] E.H. Oelkers, F. Poitrasson, Chem. Geol. 191 (2002) 73–87.
[5] A.C. Thomas, N. Dacheux, P. Le Coustumer, V. Brandel, M. Genet, J. Nucl. Mater. 281 (2000) 91–105.
[6] A.C. Thomas, N. Dacheux, V. Brandel, P. Le Coustumer, M. Genet, J. Nucl. Mater. 295 (2001) 249–264.
[7] A.C. Robisson, N. Dacheux, J. Aupiais, J. Nucl. Mater. 306 (2002) 134–146.
[8] J. Carpena, in: P. Van den Haute, F. de Corte (Eds.), Advances in Fission Track Geochronology, Kluwer Academic Press, 1998, p. 81.
[9] L.A. Boatner, B.C. Sales, in: W. Lutze, R.C. Ewing (Eds.), Radioactive Waste Forms for the Future, North-Holland Physics Publishing, Amsterdam, 1998, p. 495.
[10] J.M. Montel, S. Forest, M. Veschambre, C. Nicollet, A. Provost, Chem. Geol. 131 (1996) 37–53.
[11] M. Cuney, M. Friedrich, Bull. Miner. 110 (1987) 235–247.
[12] V. Sère, in: Géochimie des minéraux néoformés à Oklo (Gabon), histoire géologique du bassin d'Oklo: une contribution pour les études de stockages géologiques de déchets radioactifs, Thesis, Université Paris VII, Paris, 1996PA077279, 1996.
[13] R. Bros, J. Carpena, V. Sere, A. Beltritti, Radiochim. Acta 74 (1996) 277–282.
[14] B. Tissot, in: Commission Nationale d'Evaluation relative aux recherches sur la gestion des déchets radioactifs, Report no. 10, 2004, p. 46.
[15] J. Carpena, F. Audubert, D. Bernache, L. Boyer, B. Donazzon, J.L. Lacout, N. Senamaud, in: I.G. McKinley, C. McCombie (Eds.), Scientific Basis for Nuclear Waste Management XXI, Materials Research Society, 506 Keystone Drive, Warrendale, PA, USA, 1998, p. 543.
[16] O. Terra, N. Clavier, N. Dacheux, R. Podor, New J. Chem. 27 (2003) 957–967.
[17] R. Podor, M. Cuney, C. Nguyen Trung, Am. Miner. 80 (1995) 1261–1268.
[18] J.M. Montel, J.L. Devidal, D. Avignant, Chem. Geol. 191 (2002) 89–104.
[19] P. Bénard, V. Brandel, N. Dacheux, S. Jaulmes, S. Launay, C. Lindecker, M. Genet, D. Louër, M. Quarton, Chem. Mater. 8 (1996) 181–188.
[20] N. Dacheux, R. Podor, V. Brandel, M. Genet, J. Nucl. Mater. 252 (1998) 179–186.
[21] N. Dacheux, A.C. Thomas, V. Brandel, M. Genet, J. Nucl. Mater. 257 (1998) 108–117.
[22] N. Dacheux, R. Podor, B. Chassigneux, V. Brandel, M. Genet, J. Alloys Compd. 271 (1998) 236–239.
[23] A.C. Thomas in: Etude de la dissolution du phosphate diphosphate de thorium: aspect cinétique, aspect thermodynamique, Thesis, Université de Paris XI, Orsay, IPNO-T-00.09, 2000.
[24] N. Dacheux, B. Chassigneux, V. Brandel, P. Le Coustumer, M. Genet, G. Cizeron, Chem. Mater. 14 (2002) 2953–2961.
[25] V. Brandel, N. Dacheux, M. Genet, R. Podor, J. Solid State Chem. 159 (2001) 139–148.
[26] N. Clavier, N. Dacheux, P. Martinez, E. Du Fou de Kerdaniel, L. Aranda, R. Podor, Chem. Mater. 16 (2004) 3357–3366.
[27] J. Rousselle, in: Etude de la formation du phosphate diphosphate de thorium (PDT) en milieu nitrique en vue d'une décontamination d'effluents de haute activité contenant des actinides, Thesis, Université Paris XI, Orsay, IPNO-T-04.03, 2004.
[28] V. Brandel, N. Dacheux, M. Genet, in: Procédés de préparation d'un produit à base de phosphate de thorium et/ou d'uranium (IV) en vue de la décontamination d'effluents radioactifs, Patent 03739522.5-2111-FR0300426, 2003.
[29] A.L. Dragoo, Methods & Practices in X-ray Powder Diffraction, JCPDS-ICDD, vol. 6, 1992, pp. 1–6.
[30] J. Rodriguez-Carvajal, Fullprof.2k: Rietveld, profile matching and integrated intensity refinement of X-ray and neutron data, Laboratoire Léon Brillouin, CEA, Saclay, France, 2001, http://www.llb.cea.fr/fullweb/powder.htm.
[31] N.C. Nielsen, H. Bildsoe, H.J. Jakobsen, M.H. Lewitt, J. Chem. Phys. 101 (1994) 1805–1812.
[32] B.Q. Sun, P.R. Costa, D. Koscisko, P.T. Landsbury, R.G. Griffin, J. Chem. Phys. 102 (1995) 702–707.
[33] Y.K. Lee, N.D. Kurur, M. Helmle, O. Johannessen, N.C. Nielsen, M.H. Lewitt, Chem. Phys. Lett. 242 (1995) 304–309.
[34] M. Howy, H.J. Jakobsen, M. Eden, M.H. Lewitt, N.C. Nielsen, J. Chem. Phys. 108 (1998) 2686–2694.
[35] A. Bax, R. Freeman, S.P. Kempsell, J. Magn. Reson. 41 (1980) 349–353.
[36] A.C. Chapman, L.E. Thirlwell, Spectrochim. Acta 20 (1964) 937–947.
[37] S. Bruque, M.A.G. Aranda, E.R. Losilla, P. Oliveira-Pastor, P. Maireles-Tores, Inorg. Chem. 34 (1995) 893–899.
[38] D.E.C. Corbridge, J. Appl. Chem. 6 (1956) 456–465.
[39] A. Hezel, S.D. Ross, Spectrochim. Acta 22 (1966) 1949–1961.
[40] K. Nakamoto, Infrared and Raman Spectra of Inorganic and Coordination Compounds, John Wiley & Sons, New York, 1986 , pp. 106, 115, 383.

[41] P. Tarte, A. Rulmont, C. Merckaert-Ansay, Spectrochim. Acta 42A (1986) 1009–1016.
[42] A. Rulmont, R. Cahay, M. Liégeois-Duyckaerts, P. Tarte, Eur. J. Solid State Inorg. Chem. 28 (1991) 207–219.
[43] L.V. Kobets, T.A. Kolevich, D.S. Umreiko, Russ. J. Inorg. Chem. 22 (1977) 1025–1028.
[44] A.B. Yaroslavtsev, Z.N. Prozorovskaya, V.F. Chuvaev, B.F. Parshutkin, G.G. Shifanova, Russ. J. Inorg. Chem. 34 (1989) 1188–1192.
[45] M. Trchová, P. Čapková, P. Matějka, K. Melánová, L. Beněs, J. Solid State Chem. 145 (1999) 1–9.
[46] A. Hadrich, A. Lautié, T. Mhiri, F. Romain, Vib. Spectrosc. 26 (2001) 51–64.
[47] L.B. Taher, L. Smiri, A. Bulou, J. Solid State Chem. 161 (2001) 97–105.
[48] J. Emery, N. Dacheux, N. Clavier, M. Quarton, M. Genet, V. Brandel, C.R. Acad. Sci. Paris-Chimie 7 (2004) 371–375.
[49] A. Boultif, D. Louër, J. Appl. Crystallogr. 21 (1991) 987–993.
[50] A. D. Mighell, C. R. Hubbard, J. K. Stalik, NBS*AIDS83 is an expanded version of NBS*AIDS80: A Fortran Program for Crystallographic Data Evaluation, Nat. Bur. of Stand., Tech. Note 1141, 1981.
[51] V. Brandel, N. Dacheux, J. Solid State Chem. 177 (2004) 4743–4754.
[52] V. Brandel, N. Dacheux, M. Genet, Radiokhimiyia 43 (2001) 16–23.
[53] R. Hubin, P. Tarte, Spectrochim. Acta 23A (1967) 1815–1829.
[54] C.H. Huang, O. Knop, D.A. Othen, F.W.D. Woodhams, R.A. Howie, Can. J. Chem. 53 (1975) 79–91.
[55] N. Khay, A. Ennaciri, J. Alloys Compd. 323–324 (2001) 800–805.
[56] A.I. Bortun, S.A. Khainakov, L.N. Bortun, E. Jaimez, J.R. Garcia, A. Clearfield, Mat. Res. Bull. 34 (1999) 921.
[57] L. Roces, S.A. Khainakov, J.R. Garcia, P. Pertiena, M.A. Salvado, S. Garcia-Granda, Inorg. Chem. Commun. 5-9 (2002) 685.
[58] J. Emery, N. Clavier, N. Dacheux, Solid State NMR, 2005, submitted for publication.